JGR Atmospheres

RESEARCH ARTICLE
10.1029/2025JD044425

Spectral Analysis of Flickering Gamma-Ray Flashes Observed During the ALOFT 2023 Campaign

D. Sarria[1], N. Østgaard[1], I. Bjørge-Engeland[1], A. Mezentsev[1], M. Marisaldi[1,2], N. Lehtinen[1], M. Stanley[3], T. Lang[4], C. Schultz[4], and A. Fuglestad[1]

[1]Department of Physics and Technology, University of Bergen, Bergen, Norway, [2]Astrophysics and Space Science Observatory, National Institute for Astrophysics, Bologna, Italy, [3]New Mexico Institute of Mining and Technology, Socorro, NM, USA, [4]NASA Marshall Space Flight Center, Huntsville, AL, USA

Key Points:

- A detailed spectral analysis of 24 flickering gamma-ray flashes (FGF) detected by airborne lightning observatory for FEGS and TGFs (ALOFT) in July 2023 is provided
- All 24 FGFs can be fit by a relativistic runaway electron avalanche spectrum at a given location, even for low source brightnesses
- On average, ALOFT's FGFs have a source brightness about 3 orders of magnitude lower than required to be detected from space by ASIM-MXGS

Correspondence to:
D. Sarria,
david.sarria@uib.no

Citation:
Sarria, D., Østgaard, N., Bjørge-Engeland, I., Mezentsev, A., Marisaldi, M., Lehtinen, N., et al. (2025). Spectral analysis of flickering gamma-ray flashes observed during the ALOFT 2023 campaign. *Journal of Geophysical Research: Atmospheres*, *130*, e2025JD044425. https://doi.org/10.1029/2025JD044425

Received 23 MAY 2025
Accepted 30 SEP 2025

Author Contributions:
Data curation: A. Mezentsev, T. Lang, C. Schultz
Formal analysis: N. Østgaard, I. Bjørge-Engeland, A. Mezentsev, M. Marisaldi, M. Stanley, A. Fuglestad
Funding acquisition: N. Østgaard, M. Marisaldi, N. Lehtinen, T. Lang, C. Schultz
Investigation: N. Østgaard, A. Mezentsev
Methodology: N. Østgaard, A. Mezentsev, M. Stanley
Project administration: N. Østgaard, M. Marisaldi, T. Lang
Software: A. Mezentsev, M. Stanley
Validation: N. Østgaard, M. Stanley
Writing – original draft: N. Østgaard, I. Bjørge-Engeland, A. Mezentsev,

Abstract We examine a newly discovered category of high-energy radiation events called flickering gamma-ray flashes (FGF) detected during the airborne lightning observatory for FEGS and TGFs campaign in July 2023. These FGFs are characterized by highly pulsating gamma-ray emissions that have no detectable concurrent optical or radio signals (Ostgaard et al., 2024, https://doi.org/10.1038/s41586-024-07893-0). They are consistently followed by a Narrow Bipolar Event (NBE) occurring a few to 50 milliseconds after the last gamma-ray pulse. We perform a comprehensive spectral analysis of the FGFs using forward modeling and Monte Carlo simulations. We assume the NBE occurs either at the same location as the gamma-ray emission or close to it (±1 kilometer). Of 24 FGF events, we have position constraints for 21 and additional altitude constraints for 3. With sufficient photon counts, we can determine source photon brightness within a few orders of magnitude, down to one order of magnitude for some events. All FGFs are consistent with a fully developed relativistic runaway electron avalanche spectrum with varying atmospheric attenuation, even at low photon source brightnesses (10^{12} to 10^{14}, above 100 keV). FGFs are produced in the atmosphere (8–16 km altitude) with a large range of source photon brightness, from 10^{12} to about 10^{17}.We estimate they are on average 3 orders of magnitude below the ASIM-MXGS space detection threshold, though a small part of the FGF population could be detected from space. FGFs have been detected by CGRO-BATSE, and recently confirmed in ASIM data with several candidates. We encourage researchers to search for these events in data sets collected by current space, air and ground instruments.

Plain Language Summary Using high-altitude aircraft (20 km), a brand new type of hard radiation from thunderclouds was found, called "Flickering Gamma-ray Flashes" or FGFs. Unlike previously known thunderstorm radiation (TGFs, "Terrestrial Gamma-ray Flashes," primarily detected from space), that typically lasts less than a millisecond, these new FGFs: Last much longer (typically 15–250 milliseconds). Show a distinctive "flickering" pattern with multiple pulses. Do not produce visible light or radio signals when gamma-rays are emitted. Are not connected to lightning leaders. Are always followed by a strong radio signal, called a "Narrow Bipolar event" a few milliseconds after the last gamma-ray pulse. By studying 24 of these FGFs detected from 20 km altitude using Gamma-ray detectors, we found: They produce high-energy radiation up to about 30–40 MeV. They occur at various heights within clouds (8–16 km altitude). They vary greatly in brightness. They are on average about 1,000 times dimmer than TGFs detected from space. While these 24 FGFs were probably too dim to detect from space, it is possible that brighter ones exist. We encourage other researchers to look for them using current space instruments such as ASIM-MXGS and Fermi-GBM.

1. Introduction

As a result of the ALOFT flight campaign, over Florida, Central America and the Gulf of Mexico, Ostgaard et al. (2024) presented a series of observations detailing a newly identified type of gamma-ray event associated to thunderstorms, named Flickering Gamma-ray Flashes (FGFs). FGFs feature a greater number of pulses and longer durations for each pulse, compared to the multi-pulse Terrestrial Gamma-ray Flashes (TGFs), and span over a much longer time period (up to 250 milliseconds). Most importantly, they do not show any significant radio emissions happening during the gamma-ray pulses, marking a clear distinction. FGFs last between 15 and 250 ms (all pulses together), approaching the lower limit of gamma-ray glow durations (Dwyer et al., 2012; Marisaldi et al., 2024). ALOFT's findings suggest that FGFs represent a distinct type of intense radiation from thunderclouds, differing significantly from lightning-associated TGFs. In this work, we adhere to this convention;

M. Marisaldi, N. Lehtinen, M. Stanley, T. Lang, C. Schultz, A. Fuglestad
Writing – review & editing: N. Østgaard, I. Bjørge-Engeland, A. Mezentsev, M. Marisaldi, N. Lehtinen, T. Lang, C. Schultz

however, we acknowledge that other groups may define "TGF" more broadly, considering it to encompass both "FGF" and "lightning-leader-associated TGFs" as subcategories.

Initially detected by CGRO-BATSE (Dwyer, 2012; Fishman et al., 1994), FGFs were misidentified as TGFs for decades until the ALOFT campaign's discoveries in 2023 (Ostgaard et al., 2024). Spectral analysis is an effective method for investigating FGFs for several reasons. First, radio and optical signals are either non-existent or below the current instrument's threshold (noise level), making them undetectable through these means (Ostgaard et al., 2024). Second, FGFs typically generate a large number of counts on our X/gamma-ray detectors, providing large statistics for the spectral analysis. Detections of 2,000 counts or more are fairly common for these events, occurring for 9 out of 24 FGFs detected during the 60 hr of flight (about 30 hr above thunderstorms).

As far as we know, the only current candidate to explain the production of FGFs in thunderclouds is the relativistic feedback discharge (RFD) model, more specifically the version that does not necessarily require the involvement of a lightning leader (Dwyer, 2003, 2007, 2012). It does not exclude that alternative models, for example involving streamers, will be proposed in the future.

From this model it is expected for all FGF to show a fully developed Relativistic Runaway Electron Avalanche (RREA) energy spectrum (see Equation 1), and that a powerful radio event will follow FGFs. FGFs detected by ALOFT are always followed by a Narrow Bipolar Event (NBE) in radio frequencies 5–50 milliseconds after the final gamma-ray pulse, when on-board Electric Field Change Meter (EFCM) data was available. This was observed in 21 out of 24 events, with the three exceptions potentially due to EFCM being very noisy or down. In this work, we assume that this NBE is co-located or close ($<\pm 1$ km) to the location of the FGF. This is a necessary assumption to be able to constrain the FGF source photon brightness into a small enough and therefore useful altitude and radial distance intervals.

The goals of this study are to conduct a systematic spectral analysis of 24 FGF events detected by ALOFT, and evaluating individual properties: energy spectrum fit (i.e., "is RREA a good explanation?"), radial distance, altitude, and source photon brightness. First we will present the ALOFT flight campaign and the instrumentation we used for this study. Then we will present and evaluate the method used to estimate the position of the FGF and their source photon brightnesses, based on spectral analysis, Monte-Carlo modeling and location from different radio sensors. Finally, we will compare the source brightness of these FGFs with TGF observations made from space. We made our model source codes and simulation data freely available (see the Open Research section).

2. Flight Campaign and Instrumentation

In July 2023, a series of ten flights using NASA's ER-2 aircraft were conducted over thunderstorms in Florida, the Caribbean and Central America as part of the Airborne Lightning Observatory for FEGS and TGFs (ALOFT) campaign. A more detailed summary of th campaign is provided by (Lang et al., 2025). Each flight, lasting between 3 and 8 hr at an altitude of 20 km, included 3–4 hr of observation time directly above active thunderstorms. During these flights, ALOFT recorded a total of about 138 short transient gamma-ray events. This included about 100 strong or weak TGFs (which were associated with optical and/or radio emissions), 27 FGFs (emitting exclusively in X/gamma-rays), and 10 glow bursts, which are very short gamma-ray glows, lasting less than 200 milliseconds (Marisaldi et al., 2024). We kept 24 FGFs for the spectral analysis presented in this work, excluding 3 due to poor signal-to-noise ratios.

In this study, we utilize data from the Bismuth-Germanate (BGO) instrument developed by the University of Bergen (UIB-BGO). This instrument comprises three detectors, each consisting of a BGO scintillator coupled to a Photo-Multiplier Tube (PMT) with rapid readout systems. Each BGO crystal measures $15 \times 5 \times 3.2$ cm^3, for a total on-axis geometrical area of 225 cm^2. These detectors are designed to handle a wide range of count rates and the entire energy range relevant for TGFs/FGFs, from 300 keV to over 30 MeV. The architecture of the three BGO/PMT detectors is similar to one of the four High Energy Detector modules of the Modular X- and Gamma-ray Sensor (MXGS), currently in operation on the Atmosphere Space Interaction Monitor (ASIM) aboard the International Space Station (ISS) (Neubert et al., 2019; Ostgaard, Balling, et al., 2019). A more detailed presentation of the instrument set on-board ALOFT is presented in Ostgaard et al. (2024); Marisaldi et al. (2024). Based on Monte Carlo simulations, we established a 15 km radial distance limit from the aircraft's vertical projection for an aircraft altitude of 20 km. Our analysis indicates that the BGO detector (comprising three modules with 225 cm^2 geometrical area) cannot detect events further than this radius (Ostgaard et al., 2024), as

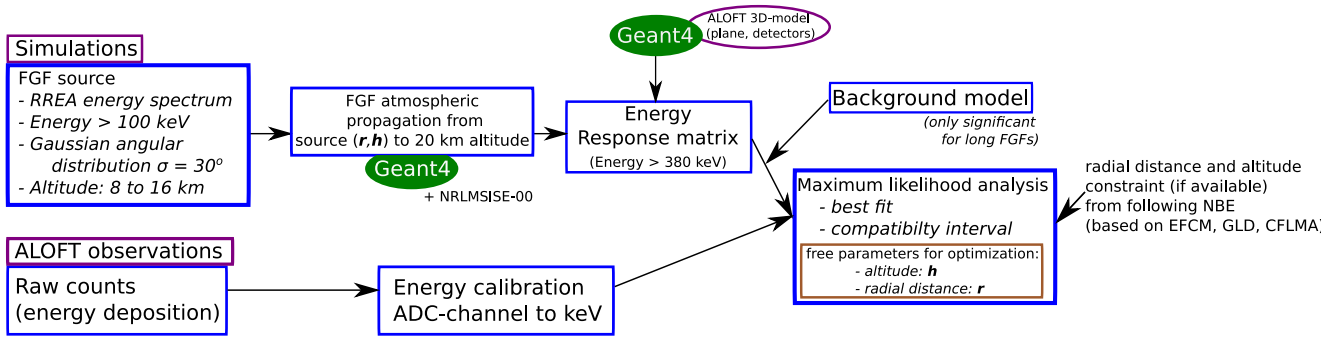

Figure 1. Description of the forward modeling approach used to perform spectral analysis on ALOFT's flickering gamma-ray flashes.

the fluence decreases by more than 5 orders of magnitude between radial distances of 0 and 15 km. This radial distance also represents the maximum range for which we could still obtain simulated low-noise energy spectra, given our available computational resources.

Since we could not establish a precise constraint on the FGF locations purely based on spectral analysis and Monte Carlo simulations, we decided to also use the location of the following NBEs, assuming they are co-located or close (within ±1 km) to the FGF gamma-rays' emission region. To constrain the NBE locations associated and following FGFs in time, three complementary instruments were used:

- EFCM (Aircraft-Based): The EFCM, mounted on the ER-2 aircraft, features a dual-channel antenna system measuring lightning-produced electric field derivatives (Quick et al., 2020). Its fast channel (10 MHz sampling, 100 μs decay) captures radiative components, while the slow channel (1 MHz sampling, 100 ms decay) measures electrostatic components. The 16-bit resolution system operates in triggered mode, capturing 1-s intervals around events. The location r (radial distance), h (altitude) is obtained using time delays from direct waves and ground reflected waves, with uncertainty intervals.
- CFLMA (Ground-Based, local): The Central Florida Lightning Mapping Array consists of six VHF stations operating in the 60–66 MHz range (Stanley et al., 2016). Each station records peak radiation events exceeding local thresholds within 80-microsecond windows at 40-nanosecond resolution. The system combines arrival times across stations to determine three-dimensional source locations and VHF powers.
- GLD360 (Ground-Based, global network): This network employs sensors in the 500 Hz–50 kHz range, combining time-of-arrival methods with magnetic direction finding (Rudlosky et al., 2017; Said & Murphy, 2016). Lightning stroke geolocation requires simultaneous detection by at least four stations. It provides an uncertainty ellipse for the horizontal location, that we use.

3. Method and Evaluation

To perform the spectral analysis of the FGF events, we use a forward modeling approach. This is illustrated in Figure 1. In a first stage, we generate a FGF following a RREA photon spectrum, sampled between 100 keV and 40 MeV:

$$S^{rrea,\gamma}(\epsilon) = \epsilon^{-1} \exp\left(-\frac{\epsilon}{\epsilon_c}\right) \text{ with } \epsilon_c = 7.3 \text{ MeV} \quad (1)$$

The simulation begins with an upward-pointing source that follows a Gaussian angular distribution with $\sigma = 30°$. While the actual value of σ for FGFs is unknown (and we do not know it is constant or not for all FGF), we adopted this value from Bjorge-Engeland et al. (2024), where it was used for weak TGFs, assuming they could have a similar angular distribution. The FGF can be approximated as a point source because simulations from the RFD model indicate a typical source horizontal extension of less than a kilometer (Dwyer, 2012), and given the spacial grid size used for this analysis, having a kilometer-wide source will not make a difference with respect to a point source.

In a second stage, the photons are propagated from source altitude h to 20 km altitude (ER-2 cruise altitude) using GEANT4 (Allison et al., 2006, 2016). It includes all the relevant processes for energetic photon, electron and

positron transport in the atmosphere. The atmospheric profile used to calculate the amtosphere in the GEANT4 model is the NRLMSISE-00 model (Picone et al., 2002). The full model is made freely available, see the Open Research section.

In the third stage, we apply the response matrix of the BGO instrument to the simulated energy spectrum, resulting in a simulated recorded spectrum. We use multiple response matrices, for each incoming angle (each combination of radial distance r and altitude h corresponds a specific incoming angle). These matrices were calculated using an updated version of the model used in Ostgaard, Christian, et al. (2019), which is also based on GEANT4. This model features a highly accurate representation of the BGO detectors and an approximate model of the surrounding material, including the pod, the ER-2 plane, and air around it (with density at 20 km altitude).

For some FGFs, the duration is long enough that background counts slightly impact the analysis. Instead of performing background subtraction on the measured spectra, we add the background into the model spectra. The added background is proportional to the total time of all pulses of the FGF, which includes all non-saturated FGF pulses and excludes intervals between pulses that only contain background counts. This duration without including background intervals (in-between pulses), referred to as "kept duration," and is presented for each FGF in Table 1. Figure 2 also illustrates how this kept duration is selected for FGF #2.

The background energy spectrum added to the model is measured precisely by the instrument during a calm period around the time of the FGF, ensuring it excludes any gamma-ray glow or any fast transient.

In the final stage of analysis, we compare the actual recorded spectra, where observed counts have been energy-calibrated, with the modeled spectra for each combination of r (radial distance) and h (altitude). This comparison employs maximum likelihood analysis (MLA), based on Poisson statistics as presented in Hauschild and Jentschel (2001). To evaluate how well a model explains an observation, we calculate the Negative Log-Likelihood (NLL), noted $\chi^2_{\lambda,P}$, as:

$$\chi^2_{\lambda,P} = 2\left[\sum_i \left(m_{r,h}(e_i) - c_i\right) - \sum_{c_i \neq 0} c_i \ln\left(\frac{m_{r,h}(e_i)}{c_i}\right)\right] \tag{2}$$

Where e_i are the energies, $m_{r,h}(e_i)$ model values (one model per $\{r,h\}$ set) at these energies, and c_i the (real) observed values. The grid used in this analysis spans altitudes h from 8 to 16 km and radial distances r from 0 to 15 km, with both dimensions incremented in steps of 1 km. Our method identifies the best fit by minimizing $\chi^2_{\lambda,P}$, that is a Negative-Log-Likelihood but also happens to follow a χ^2 statistics. It defines an accepted range of models as being below $\min\left(\chi^2_{\lambda,P}\right) + 1$, that roughly corresponds to a 1-σ error (Hauschild & Jentschel, 2001). The constraints on radial distance and altitude from the NBE following in time (if available) are applied first to reduce the parameter space before performing the MLA. This ensures that the best-fit values for r,h fall within region constrained by radio observations.

Figure 3 demonstrates a robustness test of our method using an artificially generated FGF, set with specific "wanted" altitude and radial distance parameters ($r_w = 4$ km and $h_w = 14$ km). We evaluate the method's reliability by sampling randomly $N = 100$, 500, 1,000, 5,000, 10,000, and 50,000 counts from the artificial FGF spectrum to observe if and how it converges to the predefined values of r_w and h_w.

The panels in Figure 3 shows the convergence of the maximum likelihood estimation to the correct parameters as N increases. A green cross marks the actual values of r_w and h_w, the red cross indicates the best fit, and the red contour delimitates the acceptable region for r and h values (Negative-Log-Likelihood values below the red level curve are accepted).

There is a broad acceptance range for $N = 100$ and 500, where only values at extreme high altitude and radial distance can be excluded. For context, $N < 500$ is typical for best-case ASIM TGF observations, and $N < 100$ is common for Fermi-GBM (with BGO only). The best fit is close to the actual values of r_w and h_w at $N = 1{,}000$ by coincidence, because it then deviates further when N increases to 5,000. Figure 3 shows that confining the estimations to approximately a quadrant of the parameter space requires several 1000 s of counts. To achieve a kilometer-scale accuracy in both r and h, at least $N = 50000$ counts are required. It is important to note the large uncertainty in estimating the radial distance r, which tends to be significantly larger than the uncertainty in altitude h. For instance, with $N = 5000$, the total accepted range span is approximately 5 km for h and 9 km for r.

Table 1
Summary of 24 Flickering Gamma-Ray Flashes (FGF) Detected During the ALOFT 2024 Campaign, Including Statistics From the Events, Radial Distance and Altitudes Estimates of the Following NBE (When Available)

Index	Date time (UTC)	ER-2 latitude (deg.)	ER-2 longitude (deg.)	ER-2 altitude (km)	Observed intensity	Number of counts all/ normal	Number of identified pulses	Total duration (ms)	Kept duration (ms)	GLD rad. Dist. Range (km)	EFCM alt. Range (km)
1	2023-07-06 05:08:47.300	19.20	−94.44	20.45	Medium	1,639/1,608	6	96.5	56.8	3.04–5.71	X
2	2023-07-08 05:01:12.451	12.89	−89.35	20.16	Bright, sat.	6,069/3,194	17	113.4	38.5	2.60–23.45	8.63–13.97
3	2023-07-08 05:26:21.493	12.95	−89.44	20.15	Bright, sat.	3,097/2548	8	39.8	25.3	4.86–7.45	8.85–9.2
4	2023-07-24 05:45:49.238	19.16	−94.69	20.34	Bright	3,563/2840	5	13.0	9.0	3.90–6.29	X
5	2023-07-24 06:09:27.970	19.36	−94.48	20.45	Medium	616/609	6	37.7	28.6	8.76–11.66	X
6	2023-07-24 06:43:19.640	19.25	−93.80	20.74	Bright	3,692/3,461	8	193.1	70.9	X	X
7	2023-07-24 06:55:21.650	19.26	−94.04	20.62	Bright	2170/2107	10	251.4	99.9	8.48–11.52	X
8	2023-07-24 06:55:28.868	19.27	−94.05	20.67	Bright, sat.	7,149/3,539	10	91.8	28.5	2.76–6.09	X
9	2023-07-24 06:56:07.270	19.33	−94.10	20.69	Bright	2880/2785	14	248.8	100.8	7.88–10.76	X
10	2023-07-24 07:02:22.725	19.28	−94.20	20.42	Weak	200/199	6	60.0	27.1	9.94–14.87	X
11	2023-07-24 07:02:41.534	19.27	−94.16	20.47	Bright	965/871	3	19.6	13.6	5.22–8.89	X
12	2023-07-24 07:03:14.041	19.26	−94.11	20.66	Bright	1,604/1,497	11	133.5	44.2	9.24–12.51	X
13	2023-07-24 07:03:41.869	19.25	−94.06	20.61	Weak	272/269	5	38.6	19.9	7.85–10.65	X
14	2023-07-24 07:04:10.215	19.24	−94.01	20.47	Bright, sat.	6,327/3,094	10	87.8	27.6	1.89–5.29	X
15	2023-07-24 07:06:18.667	19.19	−93.77	20.55	Bright	1,344/1,150	6	59.7	17.2	9.65–12.22	X
16	2023-07-24 07:12:41.068	19.27	−94.04	20.64	Bright	1,452/1,326	8	82.2	22.0	11.97–15.31	X
17	2023-07-24 07:13:20.208	19.33	−94.09	20.79	Bright	2432/1,625	7	57.7	16.8	9.14–13.93	X
18	2023-07-24 07:13:42.197	19.36	−94.12	20.79	Bright, sat.	4,690/2728	13	31.7	15.1	9.25–12.95	X
19	2023-07-24 07:13:52.156	19.38	−94.13	20.84	Bright	2113/2068	7	149.5	76.1	13.35–16.77	X
20	2023-07-24 07:41:32.440	19.24	−93.85	20.33	Bright	730/706	6	69.3	20.3	13.35–16.77	X
21	2023-07-24 07:43:00.805	19.18	−93.70	20.50	Bright, sat.	4,675/834	4	24.3	11.6	1.48–4.01	X
22	2023-07-26 01:41:04.633	17.40	−94.17	20.17	Weak	232/231	7	148.0	39.0	X	X

Table 1
Continued

Index	Date time (UTC)	ER-2 latitude (deg.)	ER-2 longitude (deg.)	ER-2 altitude (km)	Observed intensity	Number of counts all/ normal	Number of identified pulses	Total duration (ms)	Kept duration (ms)	GLD rad. Dist. Range (km)	EFCM alt. Range (km)
23	2023-07-26 03:10:27.115	17.70	−94.86	20.65	Weak	267/261	5	113.3	33.9	X	X
24	2023-07-29 21:03:19.950	28.69	−80.89	20.68	Bright, sat.	8,548/6,986	7	118.4	50.8	5.06–5.91	10.78–10.86
										CFLMA: 5.1	CFLMA: 10.4–10.7

Note. The location r, h of following NBE for FGF #24 was also confirmed using CFLMA. sat.: saturated. Values from CFLMA are available for FGF #24 only.

Since the source photon brightness heavily depends on r, this uncertainty leads to a variability spanning several orders of magnitude in the estimated source photons brightness, except if r, h are constrained by another method. Given the systematically large compatible intervals for r using only spectral analysis, we decided it should be also constrained from the location of the following NBE using other instruments (GLD, EFCM, CFLMA). This leads to much better estimates of the photon source brightness than would be possible with spectral analysis only.

4. Results and Discussion

In total, 27 FGFs were identified, with 24 events kept for the spectral analysis after excluding three due to poor signal-to-noise (low number of counts). Table 1 presents detailed statistics of each event, including timing, location, count rates, intensity, duration, and associated NBE location constraints. The numbering is consistent with (Ostgaard et al., 2024). Of the 24 FGFs analyzed, 21 have radial distance constraints from GLD. Three events (#2, #3, and #24) also have, in addition to GLD location, an altitude constraint from EFCM using the time difference between direct and ground reflected waves (that required first to know the radial distance from GLD, with uncertainty ellipse). A future work from the ALOFT team will present more specifically how altitude constraints based on GLD and EFCM data are estimated, and apply it for a lightning leader associated with a classical TGF event. The FGF #24 was further validated by CFLMA (it is the only one in this case). FGF #24 (2023-07-29 21:03:19.950) is actually the observationally brightest event and the BGO instrument recorded a total of 8,548 counts, comprising 6,986 "normal" counts and 1,562 "fast" counts. The distinction between "normal" and "fast" is due to the detector design. "Normal" counts are characterized by distinctly isolated PMT pulses allowing reliable energy measurement, while "fast" counts involve overlapping PMT pulses, which are pulses that are detected on top of the tail of previous pulses, introducing significant uncertainty to the energy range measurement for the second pulse; but they are real counts nonetheless. Although only normal counts are suitable for spectral analysis, all counts are used for estimating the source photon brightnesses.

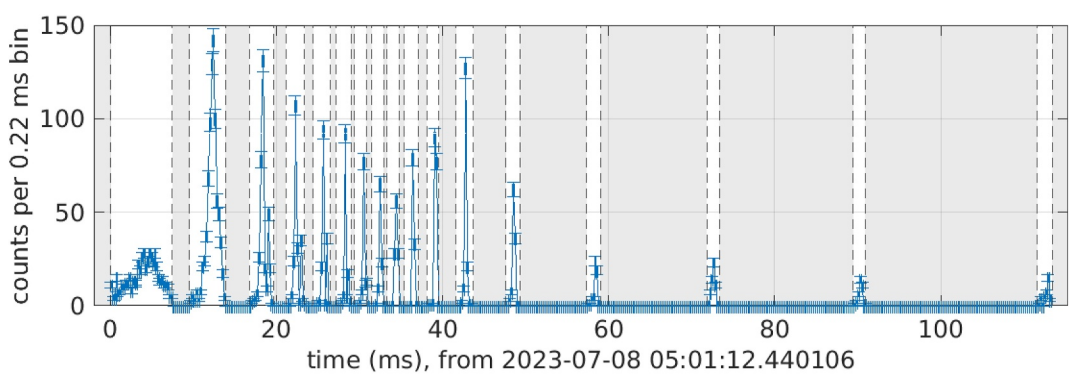

Figure 2. Detailed lightcurve of flickering gamma-ray flashes #2 (2023-07-08 05:01:12.554) recorded by the BGO detectors (summed across all detectors). This event exhibits 17 distinct peaks with a total duration of 113.4 ms, measured from the onset of the first peak to the end of the last peak. The shaded gray regions are excluded from the analysis (contain only background counts). The time interval used for spectral analysis ("kept interval," white area), here, is about 38.5 ms.

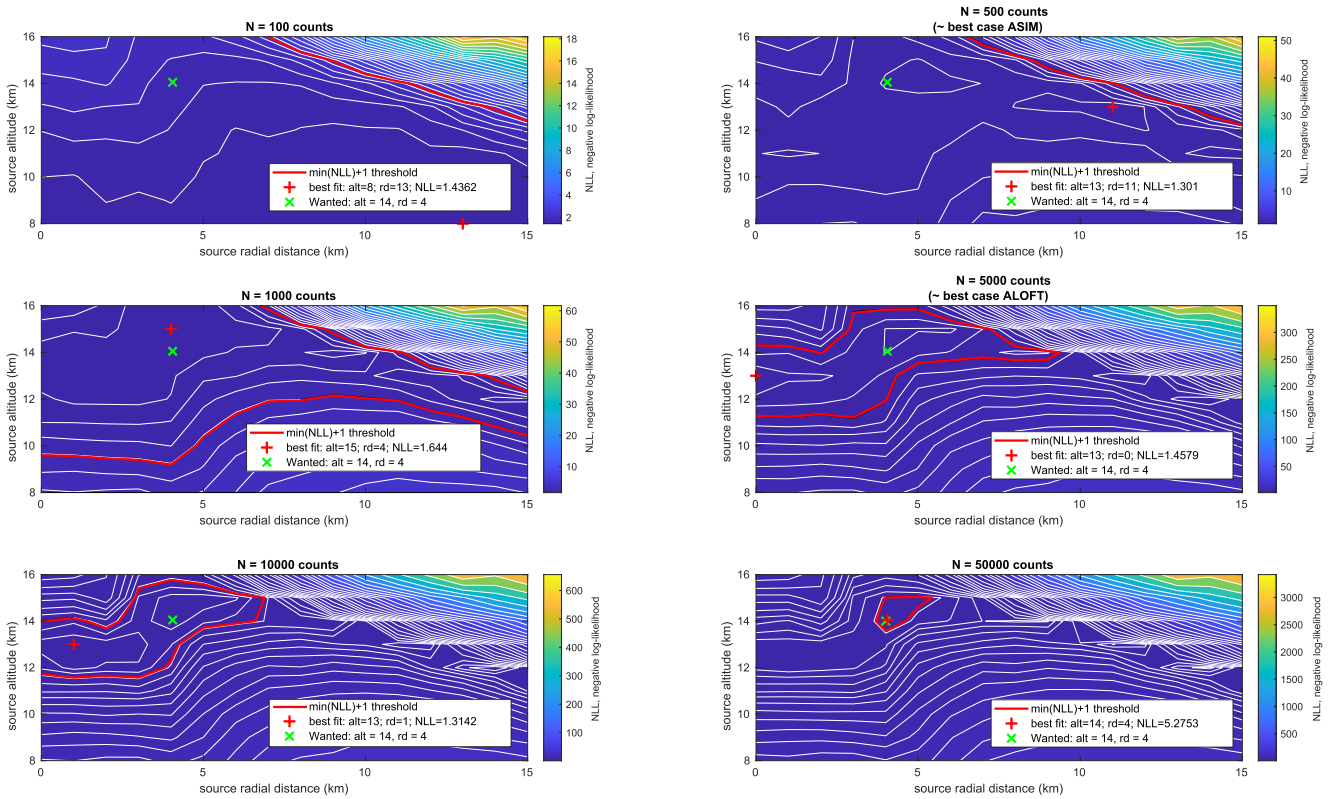

Figure 3. Test of the spectral fitting method, applying it to artificially generated observation data where the location of the flickering gamma-ray flashes is known in advance, that is "wanted" (green cross, altitude $h_w = 14$ km and radial-distance $r_w = 4$ km). The panels shows how the maximum likelihood analysis works for N randomly sampled energy counts, with $N = 100$, 500, 1,000, 5,000, 10,000 and 50,000. Here we use only simulated data.

A few FGF events, including #24 (2023-07-29 21:03:19.950, see Table 1), exhibit count saturation, which occurs when the buffers of the BGO instrument become overloaded. When it happens, only normal counts are recorded and it leads to an underestimation of the source brightness. The lightcurve of #24 and all the 24 FGFs, as well as a method to estimate how many counts could be missing, are presented in Ostgaard et al. (2024). Comparative analysis of spectra from segments with and without saturation did not show any statistical evidence of differing spectral populations.

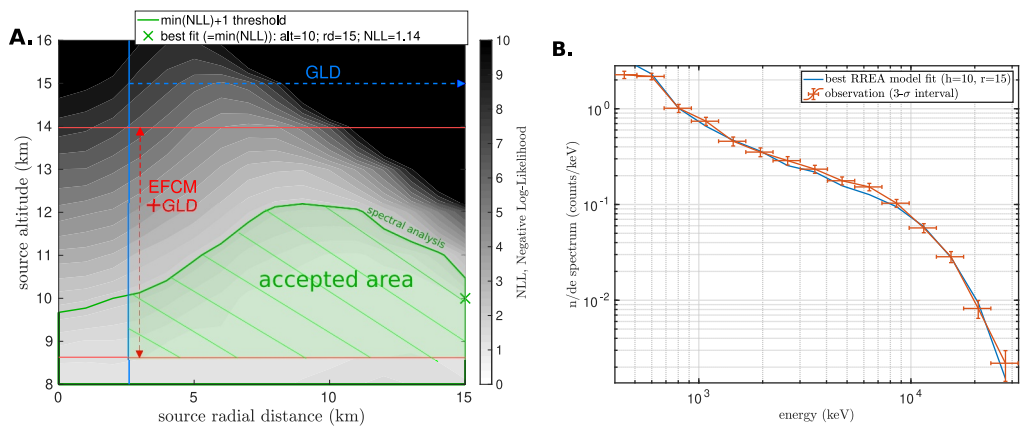

Figure 4. Example of spectral analysis result, showing flickering gamma-ray flashes #2 (2023-07-08 05:01:12.451) (a) Area of the r, h parameter space obtained from the spectral analysis, and constrains from electric field change meter and GLD. (b) Spectrum for the best fit r, h parameter set compared to the real observation by ALOFT-BGO. NLL = Negative Log-Likelihood.

Figure 4 presents one example of the MLA applied to ALOFT FGF #2 (2023-07-08 05:01:12.451). Panel (a) shows the NLL value as function of r and h. The green cross shows the best fit. The area delimited by green lines indicates the range of accepted models using the MLA only. The blue and red arrows indicate the allowed area (within uncertainty range) in both r and h based on location from GLD and EFCM. This is a good case to illustrate our method, but several cases will have much narrower r, h intervals. Some other FGF events have a constraint only on r, or only from spectral analysis. FGF #2 is characterized by a relatively low altitude with an accepted range of less than $h = 12$ km. Figure 4, Panel (b), shows the best-fit energy spectra. The event shows a very good fit qualitatively, but also quantitatively with a low NLL value (1.14). The accepted ranges of altitude and radial distances are also given in Figure 5, Panels (a) and (b).

Several FGFs showed a high count rate for individual pulses, enabling spectral analysis of each pulse individually. The maximum likelihood method consistently gave good fits for given altitude and radial distance intervals, but it was not statistically possible to distinguish a significant movement of the FGF source between pulses, based on this spectral analysis. It does not exclude the possibility that it exists, but we would need a kilometer scale or lower constrain in the analysis. That would require at least ≈50,000 counts on each FGF pulse, as discussed in previous section and shown in Figure 3.

Table 2 shows results of the MLA, including the NLL for the best fit, best fit values of r, h, and source photon brightnesses estimates for the best fit and the minimum value inside the accepted interval. All of the 24 analyzed FGFs show a good compatibility (low NLL best fit values) with a RREA spectrum coming from a given r, h location. Even if compatible photon source brightnesses go down to around 10^{12} for some events, there is no evidence of deviation from a fully developed RREA spectrum.

Figure 5, Panel (a). shows compatible altitude h intervals, Panel (b). shows the compatible radial distance r intervals, and c shows the corresponding compatible photon source brightnesses. Most of the constraints on r come from GLD (confirmed by CLMFA for FGF #24). Events #6, #19, #22, and #23 are excluded from Figure 5 as their source photon brightness estimation intervals are too wide: only FGFs with photon source brightness accepted range no larger than 4 orders of magnitude are kept in the figure.

The source photon brightness estimate is important as it enables quantitative comparisons with previous studies of TGFs detected from space (Lindanger et al., 2021; Mailyan et al., 2016, 2019). Furthermore, it helps assess the probability of detecting FGFs from space with current instruments, in particular ASIM-MXGS-BGO (Neubert et al., 2019) and Fermi-GBM-BGO (Roberts et al., 2018).

Figure 5, Panel (c), shows the source photon brightness for 20 FGF events, indicating best fits and accepted intervals. The red bars represent an estimated interval for the minimum source brightness required for each event to be detectable by ASIM-MXGS from space. For a TGF, a source photon brightness of more than a few times $\times 10^{16}$ photons above 100 keV located at 15 km altitude is usually considered detectable from space by ASIM-MXGS. In practice, the process is more complex because FGFs typically consist of multiple pulses (often around ten pulses, see FGF light-curves in Ostgaard et al. (2024)) contributing to the source brightness. Although each FGF looks different, it is common for just one of these pulses to account for about a third or a half of the total number of counts. Thus, we chose to use a rough threshold for possibility of space-based observation at approximately 10^{17} photons (above 100 keV) at 15 km altitude for the ALOFT FGFs. The values are then scaled across the range of compatible source altitudes for each FGF, accounting for atmospheric absorption between altitudes. This scaling produces the range of values shown by each of the red bars.

While the 10^{17} threshold at 15 km altitude is somewhat arbitrary (a threshold of several times 10^{16} could also be reasonable), FGFs near ASIM-MXGS's detection limit (approximately 10–20 counts) are difficult to distinguish from long TGFs based solely on their gamma-ray lightcurves.

Table 2 presents the best-fit source brightnesses at the best-fit altitude, along minimum value in the accepted interval. Considering only the best fit is not very meaningful due to the relatively large uncertainty intervals resulting from the low number of counts. These uncertainties mean the real position of the FGF could be significantly different from the best-fit location. The last column of Table 2 also shows the minimum accepted source photon brightness value.

Based on this criterion, none of the 20 FGFs would have been detectable by ASIM, with exception of FGF #2 that is an ambiguous case, with about half of the accepted range overlapping the red bar. FGFs #1 and #14 also have

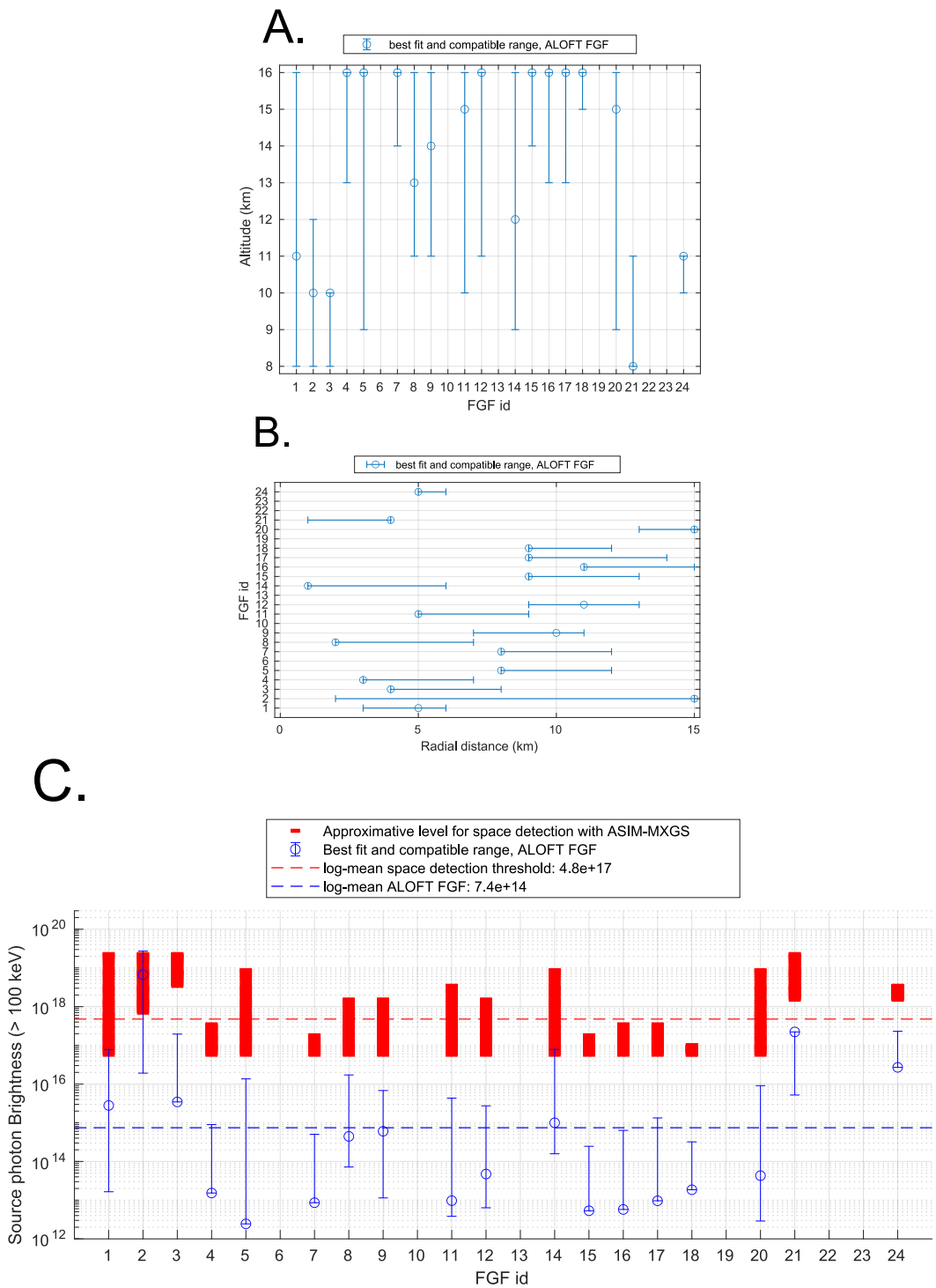

Figure 5. A Best fit altitude (circle) and accepted range (shown as error bar) of the airborne lightning observatory for FEGS and TGFs FGFs. (b) Best fit radial distance (circle) and accepted range (shown as error bar). (c) Source photon brightnesses above 100 keV, considering the best fit (circle) and compatible intervals (shown as error bar). The red bars represent the range of source photon brightnesses, scaled for different compatible source altitudes (different for any given flickering gamma-ray flashes), that would make space-based observation possible.

Table 2
Summary of the Spectral Analysis Performed on 24 Flickering Gamma-Ray Flashes (FGF) Detected During the ALOFT 2024 Campaign

Index	NLL best fit	Alt. best fit	Rad. dist. best fit	Src. γ bright. best fit	Src. γ bright. min. Accepted
1	0.30	11	5	2.80×10^{15}	1.65×10^{13}
2	1.14	10	15*	6.68×10^{18}	1.92×10^{16}
3	1.54	10	4	3.45×10^{15}	3.45×10^{15}
4	1.06	16	3	1.53×10^{13}	1.53×10^{13}
5	1.10	16	8	2.44×10^{12}	2.44×10^{12}
6	1.44	12	15*	8.55×10^{18}	3.72×10^{13}
7	1.28	16	8	8.60×10^{12}	8.60×10^{12}
8	1.17	13	2	4.44×10^{14}	7.19×10^{13}
9	1.61	14	10	6.03×10^{14}	1.14×10^{13}
10	1.17	14	13	7.53×10^{13}	7.92×10^{11}
11	0.64	15	5	9.71×10^{12}	3.82×10^{12}
12	1.24	16	11	4.73×10^{13}	6.35×10^{12}
13	0.83	16	7	1.08×10^{12}	1.08×10^{12}
14	2.22	12	1	9.97×10^{14}	1.58×10^{14}
15	2.99	16	9	5.32×10^{12}	5.32×10^{12}
16	0.98	16	11	5.75×10^{12}	5.75×10^{12}
17	1.38	16	9	9.63×10^{12}	9.63×10^{12}
18	1.66	16	9	1.86×10^{13}	1.86×10^{13}
19	1.09	16	3	1.45×10^{14}	8.37×10^{12}
20	0.76	15	15*	4.29×10^{13}	2.89×10^{12}
21	1.75	8*	4	2.22×10^{17}	5.21×10^{15}
22	1.28	14	4	8.73×10^{13}	9.19×10^{11}
23	0.69	15	4	6.19×10^{13}	1.06×10^{12}
24	3.17	11	5	2.70×10^{16}	2.70×10^{16}

Note. The analysis combines all non-saturated pulses for each individual FGF event. The spectral fitting incorporates both maximum likelihood analysis and spatial constraints derived from GLD and EFCM data, including radial distance and/or altitude estimates when available. NLL: Negati ve-Log-Likelihood. γ: gamma-ray photon. 15*: radial distance of 15 km is the maximum tested. 8*: altitude of 8 km is the minimum tested.

very small portions of their acceptable source brightness ranges touching the red bars (approximate threshold for detectability from space), but this means that the probability of ASIM detecting them during an overhead pass would have been very low.

Interestingly enough, FGF #6 coincided with an ISS (ASIM) overflight, at a quite far radial distance of 652 km (at the hedge of ASIM-MXGS field of view), but was too weak in source photon brightness, and logically did not trigger ASIM-MXGS. It happen just before the 6 weak TGF events presented in Bjorge-Engeland et al. (2024). The article presents and discusses into details the ALOFT weak TGF detections with ASIM overpass. Indeed, ALOFT also reported on a population of weak TGFs during ASIM overflights, with source brightness actually comparable to the FGFs—all below space-based detection thresholds.

On Figure 5, Panel (c), the log-mean source photon brightness for the 24 ALOFT FGFs is 7.4×10^{14} photons at the source. We chose to use this log-mean (instead of usual mean/average) because the source brightness evolves in log-scale. The log-mean of the red areas is equal to 4.8×10^{17} that is about 645 times larger, a difference of about 3 orders of magnitude.

We could try to compare these values with the findings from Lindanger et al. (2021) and Mailyan et al. (2016) for ASIM-MXGS and Fermi-BGO respectively, that provided source brightness of samples of TGFs based on spectral analysis. A correction factor of 2.4 should be applied to the data from Lindanger et al. (2021) (Figure 6 in that paper), as their measurements use a low threshold of 1 MeV for initial photons, whereas our analysis uses a 100 keV threshold. However we agreed that this approach is not satisfactory, as argued below.

The sample of TGFs used in Lindanger et al. (2021) is not representative of all the TGFs detected by ASIM, but a specific sample that was bright enough to get a good number of counts for spectral analysis, but not too bright to avoid uncorrectable instrumental effects. Converting the estimates from Mailyan et al. (2016), which use electrons at the source above 1 MeV, to photons above 100 keV is not straightforward. Mailyan et al. (2016) restricted their analysis of source electron brightness ("number of electrons") to only the best-fit results, as shown in Figure 8 of Mailyan et al. (2016). Therefore, in both cases we cannot directly compare our results to theirs estimates of source brightnesses.

Our results confirm that FGFs are substantially dimmer than classical TGFs detected from space (Ostgaard et al., 2024), explaining their very low detection probability by current space-based instruments like Fermi-GBM and ASIM-MXGS. There was an unambiguous FGF detected by ASIM on 31 May 2024 (10:36:36.160581), with 195 counts, with a few additional ambiguous candidates in the data set. In addition, an event previously presented in (Ostgaard, Neubert, et al., 2019) (Figure 8 in that paper; 22 October 2018, at 06:47:04) might also be a misidentified FGF rather than a multi-pulse Terrestrial Gamma-ray Flash (TGF). This event lacks optical (MMIA was inactive during daytime) and radio data, therefore definitive confirmation remains challenging.

FGF were also likely recorded by The Compton Gamma-Ray Observatory (CGRO), equipped with the Burst And Transient Source Experiment (BATSE) instrument: see Fishman et al. (1994) (Figure 4 in that paper) and Dwyer (2012) (Figure 11 in that paper). It had a substantial total geometrical area of 16200 cm^2, considering the 8 Large Area Detectors. TGF/FGF were also detected by the smaller Spectroscopy Detectors but not published (Dwyer et al., 2012). The instrumental effects that were important in high-flux situations, like for TGFs and FGF, were not modeled precisely for BATSE, to our knowledge. Nonetheless, the effective area is probably about an order of magnitude larger than ASIM-MXGS (total effective area ≈650 cm^2) and Fermi-GBM-BGO (total

effective area ≈320 cm^2), explaining why FGFs were more likely detected by BATSE. In addition, BATSE had a trigger window of 64 ms, which is also closer to FGF time scales.

5. Conclusions and Suggestions for Future Work

This study investigated a newly discovered class of high-energy radiation phenomena called FGF (FGFs), which were detected during the Airborne Lightning Observatory for FEGS and TGFs (ALOFT) campaign in July 2023 over tropical thunderstorms over central America, Florida and the Gulf of Mexico. Unlike traditional gamma-ray events, FGFs are characterized by the absence of concurrent optical or radio emissions. However, the last FGF pulse is most often, if not always, followed by a NBE detectable in radio frequencies.

To characterize FGF's source altitude, radial distance, and photon brightness, we developed a forward modeling approach based on Monte Carlo simulations. The initial parameter estimates from these simulations produced wide confidence intervals for photon source brightness. To constrain these intervals, we incorporated additional positional data from the following NBEs, utilizing measurements from ground detection networks (GLD360, CFLMA) and on the aircraft (EFCM).

Our analysis showed that all the 24 FGFs analyzed could be explained by a RREA spectrum coming from a range of compatible r, h locations, after going through atmospheric attenuation and detector response. This also holds for weak FGFs that could have source photon brightness down to about 10^{12}.

We then showed that all the 24 ALOFT FGFs are not sufficiently luminous to be detected from space, and are, on average, about 3 orders of magnitude weaker at source than space-detected TGF, confirming the result given in Ostgaard et al. (2024). However CGRO/BATSE very likely detected some FGFs (misidentified as classical TGFs) (Dwyer, 2012; Fishman et al., 1994), and ASIM has detected an FGF in May 2024 and has a few ambiguous candidates. Therefore it is possible that there is still a small part on a high tail of the FGF intensity distribution that could be detectable by current space instruments. Therefore we encourage the community to search for these events in data sets collected by missions that have acquired significant amounts of TGF, like ASIM-MXGS, Fermi-GBM, RHESSI or AGILE. Specifically, Fermi-GBM has an excellent absolute timing accuracy and Time-Tagged Event data. This means that every count is recorded and transmitted to the ground, unlike trigger data, which requires a minimum threshold over a given time window. The precision in timing accuracy of Fermi facilitates the temporal differentiation with the following NBE, happening typically 2–50 ms after the last FGF gamma-ray pulse. Fermi-GBM also has 12 NaI detectors (Meegan et al., 2009), that gives a total geometrical area of 1,520 cm^2, that could be used to build lightcurves and search for FGFs. Actually, Zhang et al. (2021) identified several Fermi-GBM TGF events that could potentially be FGFs, where NBEs followed TGF emissions by up to 13.5 milliseconds, though low count statistics makes it hard to distinguish more than one gamma-ray pulse.

More investigations on FGF (FGFs) could enhance our understanding of the RFD theory, currently the leading model to explain their production mechanism (Dwyer, 2012), or point us toward another mechanism. RFD seems to be a plausible explanation for phenomena observed in tropical thunderstorms, including weak TGFs, FGFs, glow bursts, and intense gamma-ray glows. If the RFD proves to play a significant role in these hard radiation events, it could also play a role in the initiation of lightning (Dwyer, 2005), at least for the class of thunderstorm that were observed during the ALOFT-2023 campaign.

Conflict of Interest

The authors declare no conflicts of interest relevant to this study.

Data Availability Statement

The model for propagation of TGF/FGF in the atmosphere (0–40 km altitude) is available on Zenodo (Sarria, 2024a). The library of FGF produced from several altitudes and detected at several radial distances are provided in Zenodo (Sarria, 2024b). The response matrices of the ALOFT BGO instrument are also available in a Zenodo repository (Sarria, 2024d). All observational data from the ALOFT July 2023 Flight campaign will be made available in the following NASA GHRC DAAC repository (Østgaard and Lang, 2025). The binned light-curves and energy spectra with best fit, for all the 24 FGF, are available in the following Zenodo repository (Sarria, 2024c).

Acknowledgments
This work made use of data from UIB-BGO, iSTORM, FEGS, EFCM, low-frequency and VHF sensors, and the Global Lightning Detection Network. The ALOFT campaign and the UIB-BGO instrument were supported by the European Research Council under the European Union's Seventh Framework Programme (FP7/2007–2013, Grant 320839) and the Research Council of Norway (Contract Nos. 223252/F50 (CoE), 325582 and 355149). This project has received funding from the European Research Council (ERC) under the European Union's Horizon Europe research and innovation programme (Grant 101201768). Some of the simulations were performed on resources provided by UNINETT Sigma2, the National Infrastructure for High Performance Computing and Data Storage in Norway (Project No. NN9526K). Work on ALOFT at the US Naval Research Laboratory is supported by the Office of Naval Research 6.1 funds. In addition,
D. Shy is supported by the US Naval Research Laboratory's Jerome and Isabella Karle Fellowship. The FEGS and EFCM team acknowledge the work of S. Podgorny, D. Corredor and M. Stewart. S.C. and Y.P. were partly supported by the National Science Foundation's Dynamic and Physical Meteorology Program (Grant AGS-2026304). The use of the VHF data was supported by the US National Science Foundation (Grant 1720600 and 2214044). A. Freeman, R. Bernath, A. Lamoureux and R. Brown of the University of Central Florida assisted with the deployment and maintenance of the VHF interferometer at the Townes Institute Science and Technology Experimentation Facility. Significant financial and logistical support for ALOFT was provided by the NASA Earth Science Division. We thank the governments of Mexico, the Bahamas, Colombia, Belize, Guatemala, Honduras, Nicaragua, Panama, the Dominican Republic, Costa Rica, El Salvador, Haiti, Turks and Caicos, Jamaica and the Cayman Islands for approving ER-2 overflights in support of ALOFT. We thank the ER-2 Project Team at NASA Armstrong Flight Research Center and the MacDill Air Force Base for acting as hosts. We warmly thank the whole ALOFT core team not included as co-authors: Eric Grove, Mason Quick, Ian Adams, Rachael Kroodsma, Gerald Heymsfield, Hugh Christian, Randall Longenbaugh, Richard Blakeslee, Phillip Bitzer, Morris Cohen, Steven Cummer, Martin Fullekrug, Joan Montanya, Marni Pazos, and Camilo Velosa. The Monte Carlo simulations were performed on resources provided by UNINETT Sigma2—the National Infrastructure for High Performance Computing and Data Storage in Norway, under project no. NN9526K, and required about 40k CPU hours.

References

Allison, J., Amako, K., Apostolakis, J., Araujo, H., Dubois, P. A., Asai, M., et al. (2006). Geant4 developments and applications. *IEEE Transactions on Nuclear Science*, *53*(1), 270–278. https://doi.org/10.1109/TNS.2006.869826

Allison, J., Apostolakis, J., Chauvie, S., Howard, A., Ivantchenko, H., Mantero, A., et al. (2016). Recent developments in geant4. *Nuclear Instruments and Methods in Physics Research Section A: Accelerators, Spectrometers, Detectors and Associated Equipment*, *835*, 186–225. https://doi.org/10.1016/j.nima.2016.06.125

Bjorge-Engeland, I., Ostgaard, N., Sarria, D., Marisaldi, M., Mezentsev, A., Fuglestad, A., et al. (2024). Evidence of a new population of weak terrestrial gamma-ray flashes observed from aircraft altitude. *Geophysical Research Letters*, *51*(17), e2024GL110395. https://doi.org/10.1029/2024GL110395

Dwyer, J. R. (2003). A fundamental limit on electric fields in air. *Geophysical Research Letters*, *30*(20), 2055. https://doi.org/10.1029/2003GL017781

Dwyer, J. R. (2005). The initiation of lightning by runaway air breakdown. *Geophysical Research Letters*, *32*(18), L20808. https://doi.org/10.1029/2005GL023975

Dwyer, J. R. (2007). Relativistic breakdown in planetary atmospheres. *Physics of Plasmas*, *14*(4), 042901. https://doi.org/10.1063/1.2709652

Dwyer, J. R. (2012). The relativistic feedback discharge model of terrestrial gamma ray flashes. *Journal of Geophysical Research*, *117*(A2), A02308. https://doi.org/10.1029/2011JA017160

Dwyer, J. R., Smith, D. M., & Cummer, S. A. (2012). High-energy atmospheric physics: Terrestrial gamma-ray flashes and related phenomena. *Space Science Reviews*, *173*(1–4), 133–196. https://doi.org/10.1007/s11214-012-9894-0

Fishman, G. J., Bhat, P., Mallozzi, R., Horack, J., Koshut, T., Kouveliotou, C., et al. (1994). Discovery of intense gamma-ray flashes of atmospheric origin. *Science-AAAS-Weekly Paper Edition-including Guide to Scientific Information*, *264*(5163), 1313–1316. https://doi.org/10.1126/science.264.5163.1313

Hauschild, T., & Jentschel, M. (2001). Comparison of maximum likelihood estimation and chi-square statistics applied to counting experiments. *Nuclear Instruments and Methods in Physics Research Section A: Accelerators, Spectrometers, Detectors and Associated Equipment*, *457*(1), 384–401. https://doi.org/10.1016/s0168-9002(00)00756-7

Lang, T. J., Østgaard, N., Marisaldi, M., Quick, M. G., Schultz, C. J., Adams, I., et al. (2025). Hunting for gamma rays above thunderstorms: The aloft campaign. *Bulletin of the American Meteorological Society*, *106*(5), 789–812. https://doi.org/10.1175/BAMS-D-24-0060.1

Lindanger, A., Marisaldi, M., Sarri, D., Østgaard, N., Lehtinen, N., Skeie, C. A., et al. (2021). Spectral analysis of individual terrestrial gamma-ray flashes detected by asim. *Journal of Geophysical Research: Atmospheres*, *126*(23), e2021JD035347. https://doi.org/10.1029/2021JD035347

Mailyan, B. G., Briggs, M. S., Cramer, E. S., Fitzpatrick, G., Roberts, O. J., Stanbro, M., et al. (2016). The spectroscopy of individual terrestrial gamma-ray flashes: Constraining the source properties. *Journal of Geophysical Research: Space Physics*, *121*(11), 11346–11363. https://doi.org/10.1002/2016ja022702

Mailyan, B. G., Xu, W., Celestin, S., Briggs, M. S., Dwyer, J. R., Cramer, E. S., et al. (2019). Analysis of individual terrestrial gamma-ray flashes with lightning leader models and fermi gamma-ray burst monitor data. *Journal of Geophysical Research: Space Physics*, *124*(8), 7170–7183. https://doi.org/10.1029/2019JA026912

Marisaldi, M., Ostgaard, N., Mezentsev, A., Lang, T., Grove, J. E., Shy, D., et al. (2024). Highly dynamic gamma-ray emissions are common in tropical thunderclouds. *Nature*, *634*(8032), 57–60. https://doi.org/10.1038/s41586-024-07936-6

Meegan, C., Lichti, G., Bhat, P. N., Bissaldi, E., Briggs, M. S., Connaughton, V., et al. (2009). The fermi gamma-ray burst monitor. *The Astrophysical Journal*, *702*(1), 791–804. https://doi.org/10.1088/0004-637X/702/1/791

Neubert, T., Østgaard, N., Reglero, V., Blanc, E., Chanrion, O., Oxborrow, C. A., et al. (2019). The ASIM mission on the international space station. *Space Science Reviews*, *215*(2), 26. https://doi.org/10.1007/s11214-019-0592-z

Ostgaard, N., Balling, J. E., Bjørnsen, T., Brauer, P., Budtz-Jørgensen, C., Bujwan, W., et al. (2019a). The modular X- and gamma-ray sensor (MXGS) of the ASIM payload on the international space station. *Space Science Reviews*, *215*(2), 23. https://doi.org/10.1007/s11214-018-0573-7

Ostgaard, N., Christian, H. J., Grove, J. E., Sarria, D., Mezentsev, A., Kochkin, P., et al. (2019b). Gamma ray glow observations at 20-km altitude. *Journal of Geophysical Research: Atmospheres*, *124*(13), 7236–7254. https://doi.org/10.1029/2019JD030312

Østgaard, N. & Lang, T. (2025). Airborne Lightning Observatory for FEGS and TGFs (ALOFT) Campaign Collection [Dataset]. *NASA EOSDIS Global Hydrometeorology Resource Center Distributed Active Archive Center*. https://doi.org/10.5067/ALOFT/DATA101

Ostgaard, N., Mezentsev, A., Marisaldi, M., Grove, J. E., Quick, M., Christian, H., et al. (2024). Flickering gamma-ray flashes, the missing link between gamma glows and tgfs. *Nature*, *634*(8032), 53–56. https://doi.org/10.1038/s41586-024-07893-0

Ostgaard, N., Neubert, T., Reglero, V., Ullaland, K., Yang, S., Genov, G., et al. (2019c). First 10 months of tgf observations by asim. *Journal of Geophysical Research: Atmospheres*, *124*(24), 14024–14037. https://doi.org/10.1029/2019JD031214

Picone, J. M., Hedin, A. E., Drob, D. P., & Aikin, A. C. (2002). NRLMSISE-00 empirical model of the atmosphere: Statistical comparisons and scientific issues. *Journal of Geophysical Research (Space Physics)*, *107*(A12), 1468. https://doi.org/10.1029/2002JA009430

Quick, M. G., Christian, H. J., Virts, K. S., & Blakeslee, R. J. (2020). Airborne radiometric validation of the geostationary lightning mapper using the fly's eye glm simulator. *Journal of Applied Remote Sensing*, *14*(4), 044518. https://doi.org/10.1117/1.JRS.14.044518

Roberts, O. J., Fitzpatrick, G., Stanbro, M., McBreen, S., Briggs, M. S., Holzworth, R. H., et al. (2018). The first fermi-gbm terrestrial gamma ray flash catalog. *Journal of Geophysical Research: Space Physics*, *123*(5), 4381–4401. https://doi.org/10.1029/2017ja024837

Rudlosky, S. D., Peterson, M. J., & Kahn, D. T. (2017). GLD360 performance relative to TRMM LIS. *Journal of Atmospheric and Oceanic Technology*, *34*(6), 1307–1322. https://doi.org/10.1175/JTECH-D-16-0243.1

Said, R., & Murphy, M. (2016). GLD360 upgrade: Performance analysis and applications. In *Proceedings of the 24th international lightning detection conference*. Retrieved from https://www.vaisala.com/sites/default/files/documents/Ryan%20Said%20and%20Martin%20Murphy.%20GLD360%20Upgrade%20Performance%20Analysis%20and%20Applications.pdf

Sarria, D. (2024a). GEANT4 model for propagation of TGF/FGF in the atmosphere (0-40 km altitude) [Software]. *Zenodo*. https://doi.org/10.5281/zenodo.15024494

Sarria, D. (2024b). Library of simulated FGF events from multiple altitudes and radial distances [Dataset]. *Zenodo*. https://doi.org/10.5281/zenodo.15349428

Sarria, D. (2024c). Binned light-curves and energy spectra with best fit for 24 FGF events [Dataset]. *Zenodo*. https://doi.org/10.5281/zenodo.15488649

Sarria, D. (2024d). Response matrices of the ALOFT BGO instrument [Dataset]. *Zenodo*. https://doi.org/10.5281/zenodo.15350194

Stanley, M. A., Rison, W., Krehbiel, P. R., Tilles, J., Liu, N., Brown, R. G., & Wilson, J. (2016). Broadband vhf interferometry within the kennedy space center lightning mapping array. In *Proceedings of the international conference on atmospheric electricity*. Retrieved from https://www.vaisala.com/sites/default/files/documents/Broadband%20VHF%20Interferometry%20withing%20the%20Kennedy%20Space%20Center_M.A.%20Stanley%20et%20al.pdf

Zhang, H., Lu, G., Lyu, F., Xiong, S., Ahmad, M. R., Yi, Q., et al. (2021). On the terrestrial gamma-ray flashes preceding narrow bipolar events. *Geophysical Research Letters*, *48*(8), e2020GL092160. https://doi.org/10.1029/2020GL092160